# TOA and AOD Statistics for Down Link Gaussian Scatterer Distribution Model

Seung-Hyun Kong, *Member, IEEE*

***Abstract*—Gaussian scatterer distribution model (GSDM) is one of the most interesting geometrically based scatterer distribution models for spatial and temporal properties of wireless channels in most multipath environments. The GSDM assumes a circular scattering region around a mobile station (MS), and the scatter density decreases with the distance from the MS. In this paper, the time of arrival (TOA), angle of departure (AOD), and joint TOA/AOD probability density functions (pdfs) of down link are derived for the GSDM. Based on these pdfs, the TOA and AOD pdfs of first arrival path are analyzed as they are particularly important to radiolocation technologies. A closed-form expression for the TOA pdf and an approximate expression for the AOD pdf of the first arrival path are obtained. To validate the closed-form expressions, comparisons to simulated normalized histograms obtained from Monte Carlo trials are included. The pdfs derived in this paper provide substantial insight into the statistical properties of wireless channels and first arrival path in multipath environments.**

***Index Terms*—Angle of departure, statistical propagation, time of arrival.**

## I. Introduction

SPACE-TIME channel model that provides accurate knowledge of time of arrival (TOA) distribution and angle of departure (AOD) distribution in multipath environments is essential to design wireless communication systems and to estimate the performance of the systems. Knowledge of the spatial and temporal properties of the received signal is necessary for the design of array antenna systems and radiolocation systems, respectively.

The literature has proposed a number of fundamental channel models with different scatterer distributions or shapes of scattering region [1]-[4] to explain the characteristics of multipath environments, and to figure out the properties of wireless multipath channels. Among these channel models, the GSDM is one of the most general models; it provides the TOA and AOD distributions that match reasonably well with field measurements [5], and it is based on a more reasonable assumption than the uniform scatterer distribution model (USDM), as the scatterers near the MS contribute more than those away from the MS [6]. As indicated in [6], the GSDM can be made suitable both for macro-cell and pico-cell environments with an appropriate choice of standard deviation of the scatterer distribution.

In [1], closed-form expressions of the up link TOA and angle of arrival (AOA) pdfs of the USDM are derived for both circular and elliptical scattering regions. The expressions for the joint TOA/AOA and marginal TOA pdfs of the USDM in [1], however, show discontinuity and algebraic singularity, respectively, when evaluating the probability density for the line of sight (LOS) path. A simplified closed-form expression for the AOA pdf of the GSDM derived in [6] indicates that the AOA pdf expression has higher validity than that in [7]. However, as discussed in [6], the AOA pdf expression derived in [6] is good for small standard deviation of the GSDM. Regarding the TOA pdf of the GSDM, an expression that requires numerical integration is provided in [6]. Pedersen *et al*. [5] suggest that the TOA pdf in urban outdoor environments roughly follows exponential distribution, which is similar to the TOA pdf of the GSDM derived in [6].

From the reciprocity of the down link to the up link, the down link TOA and AOD have distributions identical to those of the up link TOA and AOA, respectively, for a scatterer distribution model. Therefore, the joint TOA/AOD, marginal TOA, and marginal AOD pdfs of the down link correspond to the joint TOA/AOA, marginal TOA, and marginal AOA pdfs of the up link, respectively.

The purpose of this paper is to provide accurate knowledge of spatial and temporal properties of wireless channels in multipath environments based on a reasonable assumption of the scatterer distribution. This paper focuses on the GSDM around the MS as one of the most general and practical down link scatterer distributions. A second purpose of this paper is to analyze the spatial and temporal properties of the first arrival path in multipath environments. To this end, the GSDM is considered to derive the joint TOA/AOD, marginal TOA, and marginal AOD pdfs. Section II introduces definitions and notations, and Section III shows the joint TOA/AOD pdfs of the GSDM and USDM. In Section IV, the marginal TOA pdfs are derived for the GSDM and USDM. The AOD pdf is derived in Section V. In Section VI, the TOA and AOD pdfs of the first arrival path are analyzed to show the difference from those of long-delayed multipaths. A closed-form expression for the TOA pdf of the first arrival path is introduced, and an approximation of the AOD pdf of the first arrival path is discussed as well. Section VII discusses the usage of expressions derived in this paper.

## II. Down Link Geometry

Fig. 1 shows the geometry of scatterers around a MS receiving signal from a BS, and notations used in this paper to derive the TOA and AOD pdfs. The MS is at the origin $O(0,0)$, and the BS is located at $B(-D,0)$; and a circular scattering region of radius $R$ around the MS is defined in a

Manuscript received April 13, 2008; revised July 19, 2008, September 25, 2008, and November 27, 2008; accepted January 20, 2009. The associate editor coordinating the review of this paper and approving it for publication was C.-X. Wang.

S.-H. Kong is with Qualcomm Inc. (e-mail: kongseunghyun@yahoo.co.kr).

Digital Object Identifier 10.1109/TWC.2009.080508

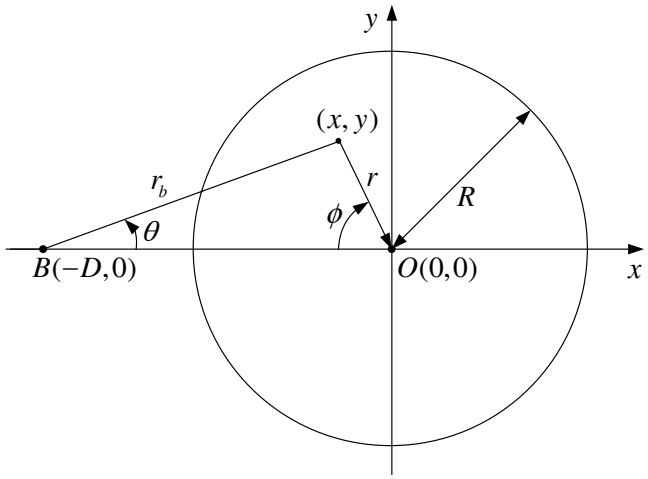


Fig. 1. Geometry of scatterer distribution.

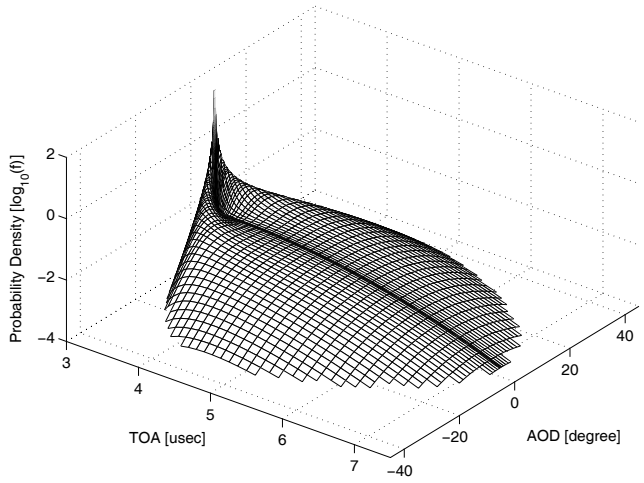


Fig. 2. Joint TOA/AOD pdf for GSDM.

Cartesian coordinate system. A down link path with AOD $\theta$ relative to the azimuth of LOS path is reflected at a scatterer located at $(x, y)$ within the scattering region and arrives at the MS on the azimuth angle $\phi$ relative to the LOS path after propagating TOA $\tau = (r_b + r)/c$ seconds, where $r_b$ is the distance to the scatterer from the BS, $r$ is the distance to the MS from the scatterer, and $c$ is the speed of light. Let $f_{x,y}(x, y)$ denote the scatterer distribution, then

$$x = r_b \cos(\theta) - D \tag{1}$$
$$y = r_b \sin(\theta) \tag{2}$$
$$\tau = (r_b + r)/c \tag{3}$$
$$r^2 = D^2 + r_b^2 - 2 r_b D \cos(\theta). \tag{4}$$

Therefore, the circular scattering region is described as

$$D^2 + r_b^2 - 2 r_b D \cos(\theta) \le R^2. \tag{5}$$

Using (3) and (4), $r_b$ can be expressed as

$$r_b = \frac{\tau^2 c^2 - D^2}{2(\tau c - D\cos(\theta))}, \tag{6}$$

and (5) becomes

$$\frac{D^2 + \tau^2 c^2 - 2\tau c D \cos(\theta)}{\tau c - D\cos(\theta)} \le 2R. \tag{7}$$

Using the Jacobian transformation in [8], the joint TOA/AOD pdf is expressed as identical to the joint TOA/AOA pdf in [1],

$$f_{\tau,\theta}(\tau, \theta) = \frac{c G_1 G_3}{4 G_2^3} f_{x,y}(r_b \cos(\theta) - D, r_b \sin(\theta)) \tag{8}$$

where

$$G_1 = \tau^2 c^2 - D^2$$
$$G_2 = \tau c - D\cos(\theta)$$
$$G_3 = D^2 + \tau^2 c^2 - 2\tau c D \cos(\theta).$$

## III. Joint TOA/AOD pdf for GSDM and USDM

Assuming the down link geometry as shown in Fig. 1, the scatterer distribution function for the GSDM is defined as

$$f_{x,y}^{G}(x, y) = \begin{cases} \frac{1}{2\pi\sigma^2} \exp[-\frac{x^2+y^2}{2\sigma^2}], & \sqrt{x^2+y^2} \le R \\ 0, & \text{otherwise} \end{cases} \tag{9}$$

where $(\cdot)^G$ denotes the GSDM, and $\sigma$, the standard deviation of the GSDM, represents multipath environments, such that larger $\sigma$ indicates wider spatial spread of scatterers around the MS. Applying (9) to (8), the joint TOA/AOD pdf for the GSDM is derived as

$$f_{\tau,\theta}^{G}(\tau, \theta) = \begin{cases} f_{\tau,\theta}^{G,1}(\tau, \theta), & \frac{G_3}{G_2} \le 2R,\ \theta \ne 0 \\ f_{\tau,\theta}^{G,2}(\tau, \theta), & D < c\tau \le (D+2R),\ \theta = 0 \\ \frac{cD}{2\pi\sigma^2}, & c\tau = D,\ \theta = 0 \\ 0, & \text{otherwise} \end{cases} \tag{10}$$

where

$$f_{\tau,\theta}^{G,1}(\tau, \theta) = \frac{c G_1 G_3}{8\pi\sigma^2 G_2^3} \exp[\frac{G_4}{8\sigma^2 G_2^2}]$$
$$f_{\tau,\theta}^{G,2}(\tau, \theta) = \frac{c(D+\tau c)}{8\pi\sigma^2} \exp[\frac{-(\tau c - D)^2}{8\sigma^2}]$$
$$G_4 = 4DG_1G_2\cos(\theta) - G_1^2 - 4D^2G_2^2$$

and $f_{\tau,\theta}^{G}(\tau, \theta)$ at the LOS ($\tau = D/c, \theta = 0$) is derived by applying L'Hospital's rule

$$\lim_{\tau \to \frac{D}{c}} f_{\tau,\theta}^{G,1}(\tau, \theta)$$

with

$$\frac{d\theta}{d\tau} = \frac{c}{D\sin(\theta)} \left(\frac{c\tau}{D} - 1\right)$$

obtained from (6) for $r_b = D$. Fig.2 shows the joint TOA/AOD pdf (10) for $D = 1000$m, $R = 600$m, $\sigma = 200$m. Similar algebraic manipulation can be applied to obtain an expression for the probability density at the LOS point of the joint up

link TOA/AOA pdf of the USDM derived in [1]; the complete closed-form expression becomes

$$f^{U}_{\tau,\theta}(\tau,\theta)=\begin{cases}\dfrac{cG_1G_3}{4\pi R^2G_2^3}, & \dfrac{G_3}{G_2}\le 2R,\ \theta\neq 0\\ \dfrac{c(D+\tau c)}{4\pi R^2}, & D<c\tau\le(D+2R),\ \theta=0\\ \dfrac{cD}{\pi R^2}, & \tau=\tau_{LOS},\ \theta=0\\ 0, & \text{otherwise}\end{cases} \tag{11}$$

where $(\cdot)^U$ denotes the USDM and $\tau_{LOS}=D/c$. Note that the joint TOA/AOD pdfs of the GSDM and USDM are continuous functions over all ranges of TOA and AOD. Note also that the joint TOA/AOD pdfs of the GSDM and USDM have two peaks at the points $(\tau_p,\pm\theta_p)$, where $\tau_p=\tau^{+}_{LOS}$ and $\theta_p=0^{+}$, and drop sharply from the peak points to the LOS point $(\tau_{LOS},0)$.

## IV. Marginal TOA pdf for GSDM and USDM

### A. GSDM

One of the approaches to derive a closed-form expression of the TOA pdf is to derive the TOA cumulative density function (cdf), and then take the derivative of the TOA cdf with respect to $\tau$. Similarly to [1], the TOA cdf can be obtained by calculating the total probability of a scatterer being inside both the ellipse corresponding to a delay equal to $\tau$ and the circular scattering region of radius $R$. However, due to the Gaussian distribution of scatterers in the circular region, the calculation requires integrals, of which the analytical evaluation is not possible [6]. The method used in this paper to derive the TOA cdf is to divide the intersection area into multiple area segments for convenience in algebraic manipulations, and then to sum up the expressions of the probabilities of a scatterer being inside each segment.

Fig. 3 shows the situations considered here. Due to the symmetry of the scatterer distribution about the $x$ axis, segments only above the $x$ axis are shown and analyzed for algebraic convenience. An arbitrary point inside the intersection area is represented by a radius $r$ from the MS located at the origin $O(0,0)$ and an angle $\phi$ increasing clockwise from the down link arrival angle of LOS path transmitted from the BS located at $B(D,0)$ in a polar coordinate system. For a TOA $\tau$, the angle to the cross section point of the circle and the ellipse is denoted by $\phi_0$, and the distance $r$ from the origin to a point on the ellipse when $\phi=\pi$ is denoted by $r_0$. The quantity $r_1$ represents the distance from the MS to the point on the ellipse, when $\phi$ is equal to an angle $\phi_1$ $(=\pi/2)$ for convenience in algebraic manipulations. Let $A_0$ denote the total circular scattering region, and let $A_{11}$, $A_{12}$, $A_{13}$, $A_{14}$ and $A_{15}$ represent area segments which constitute the intersection area above $x$ axis, over $\{0\le r\le R, 0\le\phi\le\phi_0\}$, $\{0\le r\le r_0, max(\phi_0,\phi_1)\le\phi\le\pi\}$, $\{r_0\le r\le r_1, max(\phi_0,\phi_1)\le\phi\le\pi\}$, $\{0\le r\le r_1, \phi_0\le\phi\le\phi_1\}$ and $\{r_1\le r\le R, \phi_0\le\phi\le\phi_1\}$, respectively. The total probability mass over $A_0$ is

$$\begin{aligned}V_0 &= \int_0^R 2\pi r N(r)\,dr\\ &= \sigma\sqrt{2\pi}\Big(1-\exp\big(\frac{-R^2}{2\sigma^2}\big)\Big)\end{aligned} \tag{12}$$

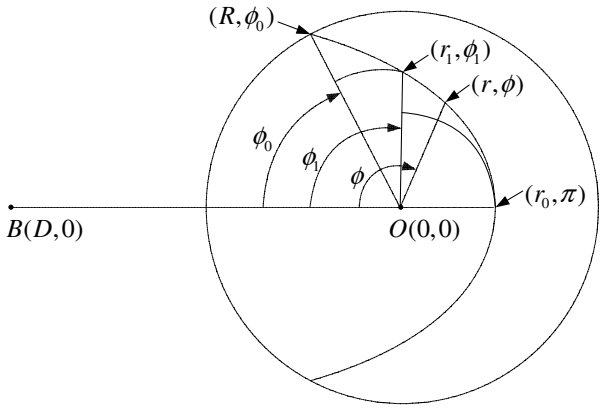


Fig. 3. Segments of the intersection area for the TOA cdf evaluation.

where

$$N(r) = \frac{1}{\sigma\sqrt{2\pi}}\exp\big(\frac{-r^2}{2\sigma^2}\big). \tag{13}$$

(14)

Since the distance from the origin to the ellipse corresponding to a delay $\tau$ is described by

$$r = \frac{\tau^2c^2-D^2}{2(\tau c-D\cos(\phi))}, \tag{15}$$

as in [1], and the $r_0$ is described by

$$r_0 = \frac{\tau c-D}{2}, \tag{16}$$

the following relationships are obtained

$$\phi_0 = \arccos\Big(\frac{D^2-\tau^2c^2+2R\tau c}{2RD}\Big) \tag{17}$$

$$r_1 = \frac{r_0(\tau c+D)}{\tau c-D\cos(\phi_1)}. \tag{18}$$

Let $\tau_1$ represent the value of $\tau$ when $\phi_0=\phi_1$,

$$\tau_1 = (R+\sqrt{R^2-2RD\cos(\phi_1)+D^2})/c, \tag{19}$$

and the probability masses over $A_{11}$, $A_{12}$, $A_{13}$, $A_{14}$ and $A_{15}$ for $\tau_1<\tau\le(D+2R)/c$ are expressed by the following equations

$$V_{11} = \frac{\phi_0}{2\pi}V_0 \tag{20}$$

$$\begin{aligned}V_{12} &= \int_0^{r_0}(\pi-\phi_0)rN(r)\,dr\\ &= \frac{\sigma}{\sqrt{2\pi}}(\pi-\phi_0)\Big(1-\exp\big(\frac{-r_0^2}{2\sigma^2}\big)\Big)\end{aligned} \tag{21}$$

$$V_{13} = \int_{r_0}^{R}(\phi-\phi_0)rN(r)\,dr \tag{22}$$

and $V_{14}=V_{15}=0$, respectively, where

$$\phi = \arccos\Big(\frac{D^2-\tau^2c^2+2r\tau c}{2rD}\Big). \tag{23}$$

To derive a closed-form expression of (22), we use an approximation [9]

$$\arccos(x) \simeq \frac{\pi}{2}-x. \tag{24}$$

Using (24), (22) is expressed as

$$V_{13} \simeq \frac{\sigma}{\sqrt{2\pi}} Z_1 (Z_4 - Z_3) + Z_2 \Big( Q(\frac{r_0}{\sigma}) - Q(\frac{R}{\sigma}) \Big) \quad (25)$$

where

$$\begin{aligned} Z_1 &= \frac{\pi}{2} - \phi_0 - \frac{\tau c}{D} \\ Z_2 &= \frac{r_0 (D + \tau c)}{D} \\ Z_3 &= 1 - \exp\big(\frac{-r_0^2}{2\sigma^2}\big) \\ Z_4 &= 1 - \exp\big(\frac{-R^2}{2\sigma^2}\big) \\ Q(x) &= \frac{1}{\sqrt{2\pi}} \int_x^\infty e^{-\frac{t^2}{2}}\, dt. \end{aligned}$$

After some algebraic manipulations, the TOA cdf for $\tau_1 < \tau \leq (D+2R)/c$ is expressed as

$$\begin{aligned} F_\tau^1(\tau) &= \frac{2}{V_0}(V_{11} + V_{12} + V_{13}) \\ &\simeq \frac{1}{2} - \frac{\tau c}{\pi D} + \big(\frac{1}{2} + \frac{\tau c}{\pi D}\big) \frac{Z_3}{Z_4} \\ &\quad + \frac{2 Z_2}{\sigma \sqrt{2\pi} Z_4} \Big( Q(\frac{r_0}{\sigma}) - Q(\frac{R}{\sigma}) \Big). \end{aligned} \quad (26)$$

Assuming $R \gg \sigma$,

$$F_\tau^1(\tau) \simeq 1 + (Z_3 - 1)\big(\frac{1}{2} + \frac{\tau c}{\pi D}\big) + \frac{2 Z_2}{\sigma \sqrt{2\pi}} Q(\frac{r_0}{\sigma}). \quad (27)$$

For $D/c < \tau \leq \tau_1$,

$$V_{12} = \frac{\sigma}{\sqrt{2\pi}} (\pi - \phi_1) Z_3 \quad (28)$$

$$V_{13} \simeq \frac{\sigma}{\sqrt{2\pi}} Z_6 (Z_5 - Z_3) + Z_2 \Big( Q(\frac{r_0}{\sigma}) - Q(\frac{r_1}{\sigma}) \Big) \quad (29)$$

$$V_{14} = \frac{\sigma}{\sqrt{2\pi}} (\phi_1 - \phi_0) Z_5 \quad (30)$$

$$V_{15} = \int_{r_1}^{R} (\phi - \phi_0) r N(r)\, dr \quad (31)$$

where

$$\begin{aligned} Z_5 &= 1 - \exp\big(\frac{-r_1^2}{2\sigma^2}\big) \\ Z_6 &= \frac{\pi}{2} - \phi_1 - \frac{\tau c}{D}. \end{aligned}$$

Since $(\phi - \phi_0) r$ in (31) decreases from $(\phi_1 - \phi_0) r_1$ to 0 as $r$ increases from $r_1$ to $R$, $(\phi - \phi_0) r$ can be roughly approximated by a first order polynomial as

$$(\phi - \phi_0) r \simeq \frac{(\phi_1 - \phi_0) r_1}{R - r_1} (R - r). \quad (32)$$

Using (32),

$$V_{15} \simeq Z_7 \left[ R \Big( Q(\frac{r_1}{\sigma}) - Q(\frac{R}{\sigma}) \Big) - \frac{\sigma}{\sqrt{2\pi}} (Z_4 - Z_5) \right] \quad (33)$$

where

$$Z_7 = \frac{(\phi_1 - \phi_0) r_1}{R - r_1}.$$

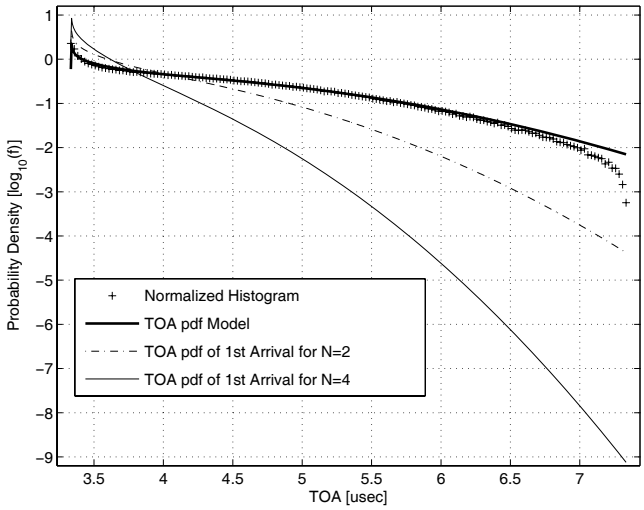


Fig. 4. TOA pdfs for GSDM.

After some algebraic manipulations, and assuming $R \gg \sigma$, the TOA cdf for $D/c < \tau < \tau_1$ is expressed as

$$\begin{aligned} F_\tau^2(\tau) &\simeq \frac{1}{\pi} \Big[ \phi_0 + \big(\frac{\pi}{2} + \frac{\tau c}{D}\big) Z_3 + Z_1 Z_5 + (Z_5 - 1) Z_7 \Big] \\ &\quad + \frac{2}{\sigma \sqrt{2\pi}} \Big[ Z_2 Q(\frac{r_0}{\sigma}) + (R Z_7 - Z_2) Q(\frac{r_1}{\sigma}) \Big]. \end{aligned} \quad (34)$$

Therefore, the complete expression of the TOA cdf becomes

$$F_\tau^G(\tau) = \begin{cases} F_\tau^1(\tau), & \tau_1 < \tau \leq (D+2R)/c \\ F_\tau^2(\tau), & D/c < \tau \leq \tau_1 \\ 0, & \text{otherwise.} \end{cases} \quad (35)$$

The closed-form expression of the TOA pdf is directly obtained by taking the derivative of (35) with respect to $\tau$

$$\begin{aligned} f_\tau^1(\tau) &\simeq c(Z_3 - 1) \Big[ \frac{1}{\pi D} - \frac{r_0}{2\pi\sigma^2} \big(\frac{\pi}{2} - 1\big) \Big] \\ &\quad + \frac{2\tau c^2}{\sigma D \sqrt{2\pi}} Q(\frac{r_0}{\sigma}) \end{aligned} \quad (36)$$

for $\tau_1 < \tau \leq (D+2R)/c$, and

$$\begin{aligned} f_\tau^2(\tau) &\simeq \frac{c}{\pi D}(Z_3 - Z_5) + \frac{(\pi - 2) r_0 c}{4\pi\sigma^2}(1 - Z_3) \\ &\quad + \frac{(1 - Z_5)}{\pi} \big(\phi_0' - Z_8\big) \\ &\quad + \frac{(1 - Z_5) Z_9}{2\pi\sigma^2} \Big[ r_0 Z_{10} (Z_1 + Z_7) + Z_2 - R Z_7 \Big] \\ &\quad + \frac{2}{\sigma\sqrt{2\pi}} \Big[ \frac{\tau c^2}{D} Q(\frac{r_0}{\sigma}) + (R Z_8 - \frac{\tau c^2}{D}) Q(\frac{r_1}{\sigma}) \Big] \end{aligned} \quad (37)$$

for $D/c<\tau\le\tau_1$, where

$$\begin{aligned}
\phi_0^{'} &= \frac{2c(\tau c-R)}{\sqrt{4R^2D^2-(D^2-\tau^2c^2+2\tau cR)^2}}\\
Z_8 &= \frac{Rc[\tau^2c^2+D^2-2D\tau c\cos(\phi_1)](\phi_1-\phi_0)}{2[R(\tau c-D\cos(\phi_1))-r_0(\tau c+D)]^2}\\
&\quad -\frac{r_0(\tau c+D)\phi_0^{'}}{R(\tau c-D\cos(\phi_1))-r_0(\tau c+D)}\\
Z_9 &= \frac{c(\tau^2c^2+D^2-2D\tau c\cos(\phi_1))}{(\tau c-D\cos(\phi_1))^2}\\
Z_{10} &= \frac{\tau c+D}{\tau c-D\cos(\phi_1)}.
\end{aligned}$$

Therefore, the complete expression of the TOA pdf becomes

$$f_\tau^G(\tau)=\begin{cases} f_\tau^1(\tau), & \tau_1<\tau\le(D+2R)/c\\ f_\tau^2(\tau), & D/c<\tau\le\tau_1\\ \dfrac{cD}{2\pi\sigma^2}, & \tau=D/c\\ 0, & \text{otherwise.}\end{cases} \tag{38}$$

Note that the probability density at LOS ($\tau=\tau_{LOS}$) in (38) is obtained from

$$\begin{aligned} f_\tau^G(D/c) &= \int_0^{2\pi} f_{\tau,\phi}^G(D/c,\phi)\,d\phi \\ &= f_{\tau,\phi}^G(D/c,0). \end{aligned} \tag{39}$$

To test the validity of the derivations, the closed-form expression of the TOA pdf in (38) is computed at all ranges of $\tau$ for $D=1000$m, $R=600$m, and $\sigma=200$m, and then compared to a simulated normalized histogram of TOA from $10^6$ times Monte Carlo trials, in Fig. 4. Note that there is a negligible, but increasing, mismatch between the TOA pdf (38) and the normalized histogram, as $\tau$ reaches to the maximum value $(D+2R)/c$ due to the approximation errors in (24) and (32).

### B. USDM

The TOA pdf for the USDM over a circular scattering region derived in [1] is strictly for $\tau>D/c$, but its probability density at LOS can be found by integrating the joint TOA/AOA pdf (11) over $\theta$ with $\tau=D/c$

$$f_\tau^U(D/c)=\int_0^{2\pi} f_{\tau,\theta}^U(D/c,\theta)\,d\theta. \tag{40}$$

Therefore, the complete expression of the TOA pdf for the USDM becomes

$$\begin{aligned} f_\tau^U(\tau) &= \frac{c}{\pi R^2}\Bigg[\frac{\tau ck_2(\pi\tau c-k_2)+(\pi k_2+\tau c-2R)k_1^2}{4k_1k_2}\\ &\quad +\frac{\tau ck_0(\tau ck_4+k_1^2)}{2k_4^2+2k_0^2k_1^2}+\frac{\tau^2c^2+k_1^2}{2k_1}\arctan\Big(\frac{k_0k_1}{k_4}\Big)\\ &\quad -\frac{R-\tau c}{\sqrt{4R^2D^2-k_3^2}}\Big(2R^2+\frac{\tau ck_1^2k_4(1+k_0^2)}{2k_4^2+2k_0^2k_1^2}\Big)\Bigg] \end{aligned} \tag{41}$$

for $D/c<\tau\le(D+2R)/c$, as derived in [1], where

$$\begin{aligned} k_0 &= \tan\Big[\frac{1}{2}\arccos\Big(\frac{D^2-\tau^2c^2+2R\tau c}{2RD}\Big)\Big]\\ k_1 &= \sqrt{\tau^2c^2-D^2}\\ k_2 &= \sqrt{D^2-\tau^2c^2+4R(\tau c-R)}\\ k_3 &= D^2-\tau^2c^2+2R\tau c\\ k_4 &= D-\tau c, \end{aligned}$$

and

$$f_\tau^U(\tau)=\frac{cD}{\pi R^2} \tag{42}$$

for $\tau=D/c$.

## V. AOD PDF FOR GSDM

To derive a closed-form expression of the AOD pdf of the GSDM, a similar approach of area segmentation used in the derivation of the TOA cdf and TOA pdf is considered. The situation being considered is illustrated in Fig. 5. The MS is at the origin $O(0,0)$ and the BS is located at $B(D,0)$ in a polar coordinate system. A down link path with AOD $\theta$ from the LOS path has two intersection points $S_1(R,\phi_1)$ and $S_2(R,\pi-\phi_2)$ with the circular scattering region of radius $R$. Let $S_3(r_3,\phi_3+\phi_1)$ be the projection of the MS to the down link path with AOD $\theta$, and $(r,2\phi_3+\phi_1-\phi)$ denotes an arbitrary point on $\overline{S_3S_2}$. The first step to derive an expression of the AOD cdf is to analyze the probabilities of a scatterer inside both the sectoral area between the LOS path and the path with AOD $\theta$ and the circular scattering region. For convenience in algebraic manipulations, 4 area segments between the angles are considered. Let $A_{21}$, $A_{22}$, $A_{23}$ and $A_{24}$ are the 4 area segments over $\{0\le r\le R,\ 0\le\phi\le\phi_1\}$, $\{0\le r\le R,\ 2\phi_3+\phi_1<\phi\le\pi\}$, $\{0\le r\le r_3,\ \phi_1<\phi\le\phi_1+\phi_3\}$ and $\{r_3\le r\le R,\ \phi_1+\phi_3<\phi\le\phi_1+2\phi_3\}$, respectively, and $A_0$ denotes the total circular scattering region. Denoting $V_0$, $V_{21}$, $V_{22}$, $V_{23}$ and $V_{24}$ the probability masses over $A_0$, $A_{21}$, $A_{22}$, $A_{23}$ and $A_{24}$, respectively,

$$\begin{aligned} V_0 &= \sigma\sqrt{2\pi}M_5\\ V_{21}+V_{22} &= \Big(\frac{1}{2}-\frac{\phi_3}{\pi}\Big)V_0 \qquad (43)\\ V_{23} &= \frac{\sigma\phi_3}{\sqrt{2\pi}}M_4 \qquad (44)\\ V_{24} &= \int_{r_3}^{R}\big[\phi_3-\arccos(\frac{r_3}{r})\big]rN(r)\,dr \qquad (45) \end{aligned}$$

where

$$\begin{aligned} \phi_3 &= \arccos\Big(\frac{D}{R}\sin(\theta)\Big)\\ r_3 &= D\sin(\theta)\\ M_4 &= 1-\exp\Big(\frac{-r_3^2}{2\sigma^2}\Big)\\ M_5 &= 1-\exp\Big(\frac{-R^2}{2\sigma^2}\Big). \end{aligned}$$

To derive a closed-form expression of (45) for $0\le\arccos(r_3/r)\le\pi/2$, an approximation [10]

$$\arccos(x)\simeq\frac{\pi}{2}-\gamma x+\frac{a_1(x+a_2)}{x+a_3} \tag{46}$$

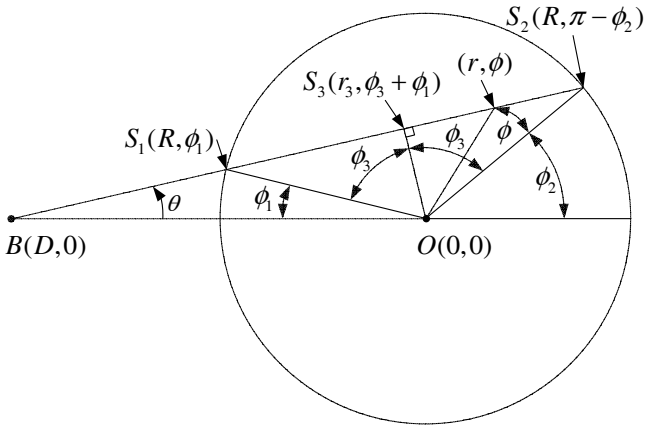


Fig. 5. Area segments for AOD cdf evaluation.

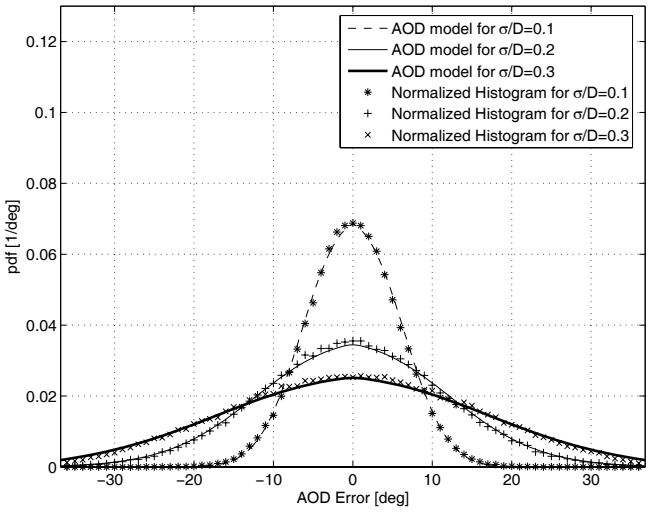


Fig. 6. AOD pdf for GSDM.

can be used if

$$\sum_{i=1}^{l}\Big|\arccos(x_i)-\big(\frac{\pi}{2}-\gamma x_i+\frac{a_1(x_i+a_2)}{x_i+a_3}\big)\Big|<\epsilon \quad (47)$$

is satisfied for a very small $\epsilon$ and for $l$ equally spaced points $\{x_i|\,0\le x_1<x_2<x_3,...<x_l\le 1, l\ge 4\}$. Using nonlinear regression with $l\gg 4$, it is found that $\gamma=0.922$, $a_1=\alpha/\beta$, $a_2=0$, and $a_3=-\beta$, where $\alpha=0.08283$ and $\beta=1.1708$, can be a choice that satisfies (47). Therefore, (45) becomes

$$\begin{aligned}V_{24} &\simeq \int_{r_3}^{R}\big[\phi_3-(\frac{\pi}{2}-\gamma\frac{r_3}{r}+\frac{\alpha r}{r_3-\beta r}+\frac{\alpha}{\beta})\big]rN(r)\,dr\\ &\simeq \int_{r_3}^{R}\big[(\phi_3-\frac{\pi}{2})r+r_3(\gamma+\frac{\alpha}{\beta^2})\big]N(r)\,dr\\ &\quad+\int_{r_3}^{R}\frac{\alpha r_3^2}{\beta^2(r\beta-r_3)}N(r)\,dr \quad (48)\end{aligned}$$

Using the first mean value theorem for integration [9], the last term in (48) can be expressed as

$$\int_{r_3}^{R}\frac{\alpha r_3^2}{\beta^2(r\beta-r_3)}N(r)\,dr \quad (49)$$

$$\le \frac{\alpha r_3^2}{\sigma\beta^3\sqrt{2\pi}}(1-M_4)\ln\big(\frac{R-\xi}{r_3-\xi}\big) \quad (50)$$

$$\ge \frac{\alpha r_3^2}{\sigma\beta^3\sqrt{2\pi}}(1-M_5)\ln\big(\frac{R-\xi}{r_3-\xi}\big) \quad (51)$$

where $\ln(\cdot)$ is a natural log function, and $\xi=r_3/\beta$. Since the upper limit (50) is negligibly small for all $\theta$, and the lower limit (51) approaches to 0 for large $R/\sigma$, as a rule of thumb, (49) can be approximated by

$$\frac{\alpha r_3^2}{2\sigma\beta^3\sqrt{2\pi}}(1-M_4)\ln\big(\frac{R-\xi}{r_3-\xi}\big). \quad (52)$$

The total probability mass can be expressed as

$$\begin{aligned}P(\theta) &= \frac{1}{V_0}(V_{21}+V_{22}+2V_{23}+2V_{24})\\ &\simeq \frac{M_4}{2M_5}+\frac{r_3}{2\pi\sigma M_5}\bigg[\frac{\alpha r_3}{\sigma\beta^3}(1-M_4)\ln\big(\frac{R-\xi}{r_3-\xi}\big)\\ &\quad+2\sqrt{2\pi}\big(\gamma+\frac{\alpha}{\beta^2}\big)\Big(Q\big(\frac{r_3}{\sigma}\big)-Q\big(\frac{R}{\sigma}\big)\Big)\bigg]. \quad (53)\end{aligned}$$

Therefore, the AOD cdf can be expressed, in terms of (53), as

$$F_\theta^G(\theta)=\begin{cases}0.5+P(\theta), & 0\le\theta\le\theta_{max}\\ 0.5-P(|\theta|)\,, & -\theta_{max}\le\theta<0\\ 0, & \text{otherwise}\end{cases} \quad (54)$$

where $\theta_{max}=\arcsin(R/D)$. Taking derivative of (53) with respect to $\theta$,

$$\begin{aligned}p(\theta) &\simeq \frac{2D\cos(\theta)}{\sqrt{2\pi}\sigma M_5}\big(\gamma+\frac{\alpha}{\beta^2}\big)\Big(Q\big(\frac{r_3}{\sigma}\big)-Q\big(\frac{R}{\sigma}\big)\Big)\\ &\quad+\frac{r_3D\cos(\theta)}{2\pi\sigma^2M_5}(1-M_4)\bigg[\pi-2\big(\gamma+\frac{\alpha}{\beta^2}\big)\\ &\quad+\frac{\alpha}{\beta^3}\Big(\big(2-\frac{r_3^2}{\sigma^2}\big)\ln\big(\frac{R-\xi}{r_3-\xi}\big)+\frac{R}{\xi-R}\Big)\bigg], \quad (55)\end{aligned}$$

and the AOD pdf can be expressed, in terms of (55), as

$$f_\theta^G(\theta)=\begin{cases}p(|\theta|), & 0<|\theta|\le\theta_{max}\\ \dfrac{D}{\sqrt{2\pi}\sigma M_5}\big(\gamma+\dfrac{\alpha}{\beta^2}\big)\big[1-2Q\big(\dfrac{R}{\sigma}\big)\big], & \theta=0\\ 0, & \text{otherwise.}\end{cases} \quad (56)$$

When $R\gg\sigma$ is assumed, (55) may be further simplified since $M_5\simeq 1$ and $Q\big(R/\sigma\big)\simeq 0$. To test the validity of the derivations, (56) is computed for all ranges of $\theta$ for $\sigma=100$m, 200m, and 300m, when $D=1000$m and $R=600$m, and then compared with simulated normalized histograms of AOD from $10^5$ Monte Carlo trials, in Fig. 6. Unlike the expressions for the up link AOA distribution of the GSDM derived in [6] and [7], (56) matches the simulated normalized histogram for small and large values of $\sigma$.

## VI. TOA and AOD Statistics of First Arrivals

The TOA pdf (38) and AOD pdf (56) describe the temporal and spatial properties of wireless channels in multipath environments. What's more, for some wireless systems, the temporal and spatial properties of first arrival path are also particularly important for an accurate estimation of performance. Direction finding systems [2] and radiolocation systems such

as Advanced Forward Link Trilateration (AFLT) [11] and Observed Time Difference of Arrival (O-TDOA) [12] use the measurement of the first arrival path to improve accuracy. In practice, a number of multipaths can be observed at a wireless receiver, and the first arrival path may have different TOA and AOD distributions from the TOA pdf (38) and AOD pdf (56). The TOA and AOD pdfs of the first arrival path have normally narrower distribution than the TOA and AOD pdfs of all multipaths [13]. Therefore, the knowledge of the temporal and spatial properties of the first arrival path is essential for the design and improvement of the radiolocation and direction finding systems, respectively. This section discusses closed-form expressions for the TOA and AOD pdfs of the first arrival path.

In [13], the TOA distribution of the first arrival path when $N$ multipaths are observed is derived as

$$f^G_{\tau_{(1)}}(\tau) \;=\; N[1-F^G_\tau(\tau)]^{N-1} f^G_\tau(\tau) \tag{57}$$

where $\tau_{(1)}$ is the first order statistic of $\tau$'s, and $F^G_\tau(\tau)$ and $f^G_\tau(\tau)$ are defined in (35) and (38), respectively. Plots in Fig. 4 include the TOA pdfs of first arrival path for $N = 2$ and 4, when $D = 1000$m, $R = 600$m, and $\sigma = 200$m. As shown in Fig. 4, the probability density around the LOS path ($\tau \simeq \tau_{LOS}$) increases linearly with $N$, but the probability density at large delay ($\tau \gg \tau_{LOS}$) decreases as $N$ increases. Therefore, it is obvious that $\tau_{(1)}$ approaches to $\tau_{LOS}$ as $N$ increases

$$\begin{aligned} E[\tau_{(1)}] \;&=\; \int_0^\infty \tau N[1-F^G_\tau(\tau)]^{N-1} f^G_\tau(\tau)\, d\tau \\ &\to\; \tau^+_{LOS}, \quad \text{as } N\to\infty. \end{aligned} \tag{58}$$

The AOD distribution of the first arrival path is defined in [13] as

$$\begin{aligned} f^G_{\theta_{\tau_{(1)}}}(\theta) \;&=\; \int_0^\infty f^G_{\theta|\tau}(\theta|\tau) f^G_{\tau_{(1)}}(\tau)\, d\tau \\ &=\; \int_{\tau_1(\theta)}^{\tau_2(\theta)} N[1-F^G_\tau(\tau)]^{N-1} f^G_{\tau,\theta}(\tau,\theta)\, d\tau \end{aligned} \tag{59}$$

where $\theta_{\tau_{(1)}}$ denotes the AOD of the first arrival path, $f^G_{\tau,\theta}(\tau,\theta)$ is defined in (10), and $\tau_1$ and $\tau_2$ represent the TOA's at the $S_1$ and $S_2$ points in Fig.5, respectively

$$\tau_1 = \left[R + D\cos(\theta) - \sqrt{D^2(\cos(\theta)^2-1)+R^2}\,\right]/c \tag{60}$$

$$\tau_2 = \left[R + D\cos(\theta) + \sqrt{D^2(\cos(\theta)^2-1)+R^2}\,\right]/c. \tag{61}$$

Note that it is not possible to obtain a closed-form expression from (59) for all values of $N$. However, it can be inferred that (59) has probability density increase relatively more at smaller $|\theta|$ as $N$ increases : The peak density of $f^G_{\theta_{\tau_{(1)}}}(\theta)$,

$$f^G_{\theta_{\tau_{(1)}}}(\theta_p) \;\simeq\; \int_{\tau_{LOS}}^{\frac{D+2R}{c}} N[1-F^G_\tau(\tau)]^{N-1} f^G_{\tau,\theta}(\tau,\theta_p)\, d\tau,$$

increases as $N$ increases, where $\pm\theta_p$ is the AOD of the peak points of the joint TOA/AOD pdf (10), since both $[1-F^G_\tau(\tau)]$ and $f^G_{\tau,\theta}(\tau,\theta_p)$ are monotonously decreasing functions with respect to $\tau(>\tau_{LOS})$. In addition, the density ratio of $f^G_{\theta_{\tau_{(1)}}}(\theta)$ to the peak,

$$\frac{f^G_{\theta_{\tau_{(1)}}}(\theta)}{f^G_{\theta_{\tau_{(1)}}}(\theta_p)} \;\simeq\; \frac{\int_{\tau_1(\theta)}^{\tau_2(\theta)} [1-F^G_\tau(\tau)]^{N-1} f^G_{\tau,\theta}(\tau,\theta)\, d\tau}{\int_{\tau_{LOS}}^{\frac{D+2R}{c}} [1-F^G_\tau(\tau)]^{N-1} f^G_{\tau,\theta}(\tau,\theta_p)\, d\tau},$$

decreases as $|\theta|(>\theta_p)$ increases and as $N$ increases, since $f^G_{\tau,\theta}(\tau,\theta)$ is a monotonously decreasing function with respect to $\tau(>\tau_{LOS})$ and $|\theta|(>\theta_p)$. Denoting the AOD of smallest magnitude among $N$ AOD values of $N$ multipaths by $\theta_{(1)}$, the pdf of $\theta_{(1)}$ can be defined as

$$f^G_{\theta_{(1)}}(\theta) \;=\; N[1-2P(|\theta|)]^{N-1} f^G_\theta(\theta). \tag{62}$$

It can be inferred from (62) that $f^G_{\theta_{(1)}}(0)$ increases linearly as $N$ increases, since

$$f^G_{\theta_{(1)}}(0) \;=\; N f^G_\theta(0),$$

and that the density ratio of $f^G_{\theta_{(1)}}(\theta)$ to the peak,

$$\frac{f^G_{\theta_{(1)}}(\theta)}{f^G_{\theta_{(1)}}(0)} \;=\; [1-2P(|\theta|)]^{N-1} \frac{f^G_\theta(\theta)}{f^G_\theta(0)},$$

decreases as $|\theta|$ increases and as $N$ increases, since $P(|\theta|)$ is a monotonously increasing function with respect to $|\theta|$. Numerical evaluations of (59) and (62) shows that both $f^G_{\theta_{\tau_{(1)}}}(\theta)$ and $f^G_{\theta_{(1)}}(\theta)$ have a similar but not identical pattern of density change when $N$ increases. However, it is expected that

$$\begin{aligned} \sigma_{\theta_{(1)}} \;&\le\; \sigma_{\theta_{\tau_{(1)}}} \\ f^G_{\theta_{(1)}}(0) \;&\ge\; f^G_{\theta_{\tau_{(1)}}}(\theta_p) \end{aligned}$$

for $N>1$, where $\sigma_{\theta_{(1)}}$ and $\sigma_{\theta_{\tau_{(1)}}}$ denote the standard deviation of $\theta_{(1)}$ and $\theta_{\tau_{(1)}}$, respectively. Let $m$ be the peak density ratio of $f^G_{\theta_{\tau_{(1)}}}(\theta)$ to $f^G_{\theta_{(1)}}(\theta)$ such that

$$m \;\simeq\; \frac{\int_{\tau_{LOS}}^{\frac{D+2R}{c}} [1-F^G_\tau(\tau)]^{N-1} f^G_{\tau,\theta}(\tau,\theta_p)\, d\tau}{f^G_{\theta_{(1)}}(0)}, \tag{63}$$

$m$ approaches a constant value as $N\to\infty$, since

$$\begin{aligned} &\int_{\tau_{LOS}}^{\frac{D+2R}{c}} [1-F^G_\tau(\tau)]^{N-1} f^G_{\tau,\theta}(\tau,\theta_p)\, d\tau\Big|_{N\to\infty} \\ &\to f^G_{\tau,\theta}(\tau_p,\theta_p). \end{aligned} \tag{64}$$

Fig. 7 shows $m$ (63) from simulated normalized histograms of $10^7$ Monte Carlo trials for $\sigma/D = 0.1, 0.2$, and $0.3$, when $D$ = 1000m and $R$ = 600m. As expected from (64), $m$ approaches a constant value for each $\sigma/D$ value when $N$ becomes sufficiently large. However, it should be noted that the plots in Fig. 7 show approximate estimates of $m$ as they are the results of Monte Carlo trials. Fig. 8 also shows the ratio $\sigma_{\theta_{\tau_{(1)}}}/\sigma_\theta$ and $\sigma_{\theta_{(1)}}/\sigma_\theta$, where $\sigma_\theta$ denotes the standard deviation of AOD $\theta$ described in (56). Note that there can be an interesting observation about the relationship between $f^G_{\theta_{\tau_{(1)}}}(\theta)$ and $f^G_{\theta_{(1)}}(\theta)$ from Fig. 7 and Fig. 8; when $f^G_{\theta_{(1)}}(\theta)$ from $M$ multipaths and $f^G_{\theta_{\tau_{(1)}}}(\theta)$ from $N$ multipaths have a same peak value, both of the pdfs also have similar standard deviation values. For example, the peak value of $f^G_{\theta_{\tau_{(1)}}}(\theta)$ for

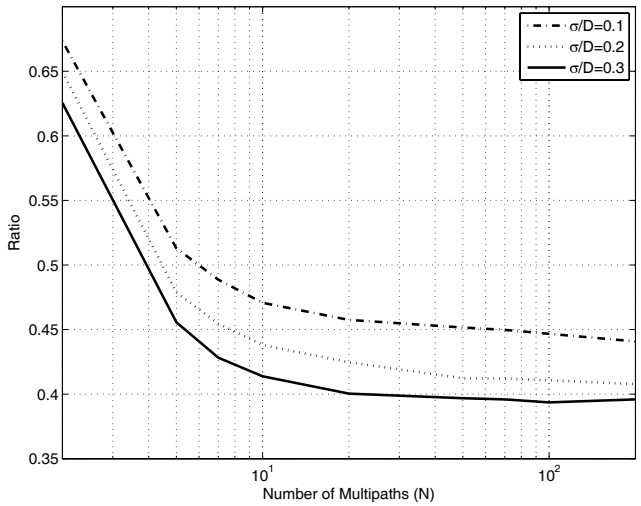


Fig. 7. Peak density ratio of $\theta_{\tau_{(1)}}$ to $\theta_{(1)}$.

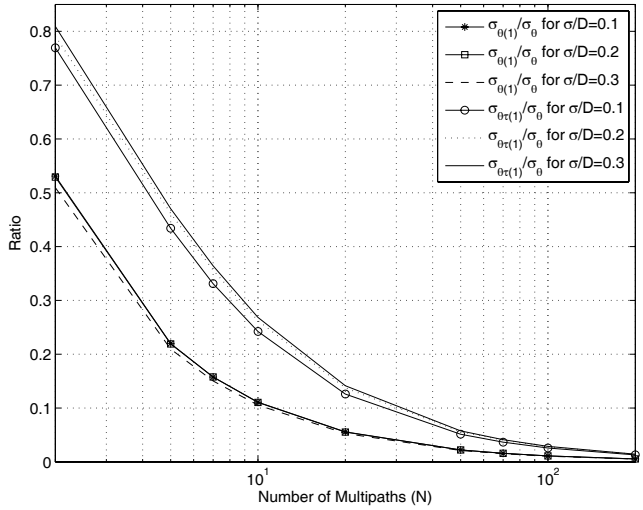


Fig. 8. Ratio of $\sigma_{\theta_{\tau_{(1)}}}/\sigma_\theta$ and $\sigma_{\theta_{(1)}}/\sigma_\theta$.

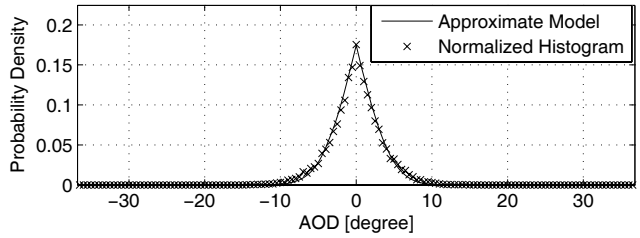


(a) $N=5$, $\sigma/D=0.1$

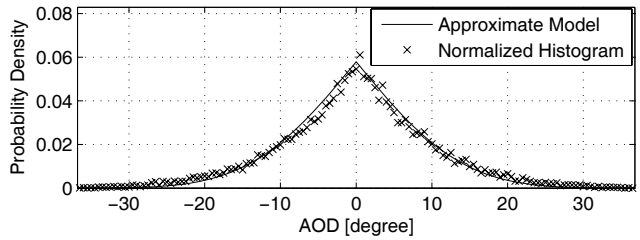


(b) $N=5$, $\sigma/D=0.3$

Fig. 9. AOD pdf of first arrival path when $N=5$.

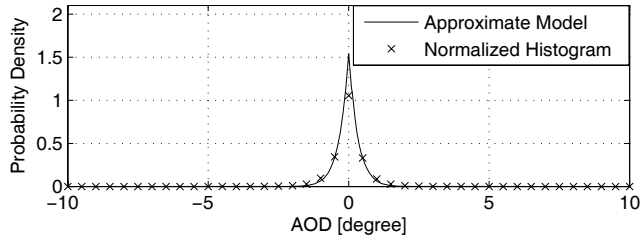


(a) $N=50$, $\sigma/D=0.1$

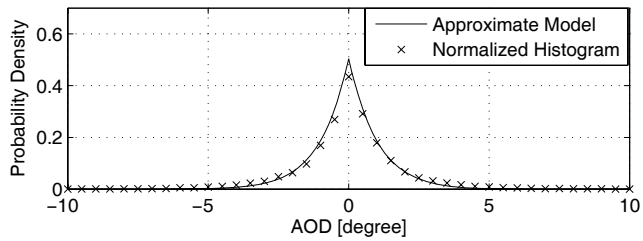


(b) $N=50$, $\sigma/D=0.3$

Fig. 10. AOD pdf of first arrival path when $N=50$.

$N = 20$ and $\sigma/D = 0.3$ is approximately same to that of $f^G_{\theta_{(1)}}(\theta)$ for $M \simeq 8$ and $\sigma/D = 0.3$ as shown in Fig. 7, and $\sigma_{\theta_{\tau_{(1)}}}$ for $N=20$ and $\sigma/D=0.3$ is also approximately same to $\sigma_{\theta_{(1)}}$ for $M \simeq 8$ and $\sigma/D=0.3$ as shown in Fig. 8. Based on the above analysis and numerical evaluations, $f^G_{\theta_{\tau_{(1)}}}(\theta)$ from $N$ multipaths can be roughly approximated by $f^G_{\theta_{(1)}}(\theta)$ from $M(<N)$ multipaths such that

$$f^G_{\theta_{\tau_{(1)}}}(\theta) \approx mN[1-2P(|\theta|)]^{mN-1} f^G_\theta(\theta). \qquad (65)$$

Fig. 9 and Fig. 10 show some comparisons of the approximation of $f^G_{\theta_{\tau_{(1)}}}(\theta)$ (65) to $f^G_{\theta_{\tau_{(1)}}}(\theta)$ (59) obtained from simulated normalized histogram of $10^6$ Monte Carlo trials. Fig. 9 (a) shows $f^G_{\theta_{\tau_{(1)}}}(\theta)$ (59) from simulated normalized histogram for $N = 5$ and $\sigma/D = 0.1$ and the approximation of $f^G_{\theta_{\tau_{(1)}}}(\theta)$ (65) using $m \approx 0.51$ from Fig. 7. Fig. 9 (b) shows another comparison for $N = 5$ and $\sigma/D = 0.3$ using $m \approx 0.46$ from Fig. 7. Fig. 10 (a) shows a third comparison for $N=50$ and $\sigma/D = 0.1$ using $m \approx 0.45$ from Fig. 7, and Fig. 10 (b) shows the other comparison for $N=50$ and $\sigma/D=0.3$ using $m \approx 0.40$ from Fig. 7. As shown in Fig. 9 and Fig. 10, (65) is effective as a coarse approximation. However, it should be noted that there is an approximation error in (65) for large $N$ and small $\sigma/D$, since the numerical evaluation of $m$ from Monte Carlo trials loses accuracy for larger N and smaller $\sigma/D$ due to too narrow bin size; Fig. 10 shows an example of this approximation error.

## VII. Conclusion

In this paper, the closed-form expressions for the joint TOA/AOD, marginal TOA, and marginal AOD pdfs of the GSDM were derived, and the validity of the TOA and AOD pdfs was confirmed by comparing the pdfs to the simulated normalized histograms from numerous Monte Carlo trials. The TOA pdf of the first arrival path and the AOD pdf of the smallest AOD magnitude path were derived from the first order

statistic of the TOA and AOD of the GSDM, respectively. It was shown that there were statistical similarities between the AOD pdf of the first arrival path and the AOD pdf of smallest AOD magnitude path with smaller number of multipaths; further mathematical analysis to derive an accurate relationship between the two pdfs will provide more insight into the spatial properties of the first arrival path. The expressions derived in this paper can be very useful for performance simulations of wireless communication systems, radiolocation systems, and direction finding systems in multipath channel environments.

## ACKNOWLEDGMENT

The author would like to thank the reviewers for helpful suggestions.

## REFERENCES

[1] R. B. Ertel and J. H. Reed, "Angle and time of arrival statistics for circular and elliptical scattering models," *IEEE J. Select. Areas Commun.*, vol. 17, pp. 1829-1840, Nov. 1999.

[2] P. Petrus, J. H. Reed, and T. S. Rappaport, "Geometrically based statistical channel model for macrocellular mobile environments," in *Proc. IEEE GLOBECOM*, 1996, pp. 1197-1201.

[3] W. C. Jakes, *Microwave Mobile Communications*. New York: Wiley, 1974.

[4] F. Fuhl, A. F. Molisch, and E. Bonek, "Unified channel model for mobile radio systems with smart antennas," *IEE Proc. Radar, Sonar, Navig.*, vol. 145, pp. 32-41, Feb. 1998.

[5] K. I. Pedersen, P. E. Mogensen, and B. H. Fleury, "A stochastic model of the temporal and azimuthal dispersion seen at the base station in outdoor propagation environments," *IEEE Trans. Veh. Technol.*, vol. 49, pp. 437-447, Mar. 2000.

[6] R. Janaswamy, "Angle and time of arrival statistics for the Gaussian scatter density model," *IEEE Trans. Wireless Commun.*, vol. 1, pp. 488-497, July 2002.

[7] M. P. Lötter and P. van Rooyen, "Modeling spatial aspects of cellular CDMA/SDMA systems," *IEEE Commun. Lett.*, vol. 3, pp. 128-131, May 1999.

[8] A. Papoulis, *Probability, Random Variables and Stochastic Processes*, 3rd ed. New York: McGraw-Hill, 1991.

[9] E. Kreyszig, *Advanced Engineering Mathematics*, 9th ed. John Wiley & Sons, 2006.

[10] S. Huet, A. Bouvier, M.-A. Poursat and E. Jolivet, *Statistical Tools for Nonlinear Regression: A Practical Guide with S-PLUS and R Examples*, 2nd ed. New York: Springer-Verlag, 2003.

[11] TIA/EIA IS-801-1, Position Determination Service Standards for Dual-Mode Spread Spectrum Systems-Addendum, Mar. 2001.

[12] 3GPP TS 25.305, Stage 2 functional specification of UE positioning in UTRAN, V4.7.0, Dec. 2003.

[13] S.-H. Kong, "Advancements in mobile positioning technologies and mobile location networks," Ph.D. dissertation, Stanford Univ., Stanford, CA 94305, 2006.

**Seung-Hyun Kong** received a B.S.E.E. from Sogang University, Korea, in 1992, an M.S.E.E. from Polytechnic University, New York, in 1994, and a Ph.D. degree in Aeronautics and Astronautics from Stanford University, CA, in 2006. From 1997 to 2000, he was a research member for CDMA standard development and mobile position location technology at Samsung Electronics, Inc., Korea. From 2000 to 2004, he worked for Nexpilot Inc., Korea, as an R&D lead for UMTS location system development. In 2006, he worked for Polaris Wireless, Inc., where he was involved with hybrid positioning technology development using wireless location signature system and Assisted GPS. Since 2007, he is with Qualcomm, Inc., San Diego, where he works for indoor location technology research and development. His research interests include mobile location technologies such as A-GPS and AFLT, modeling statistical propagation of wireless channels, and signal detection algorithms in wireless communication systems.